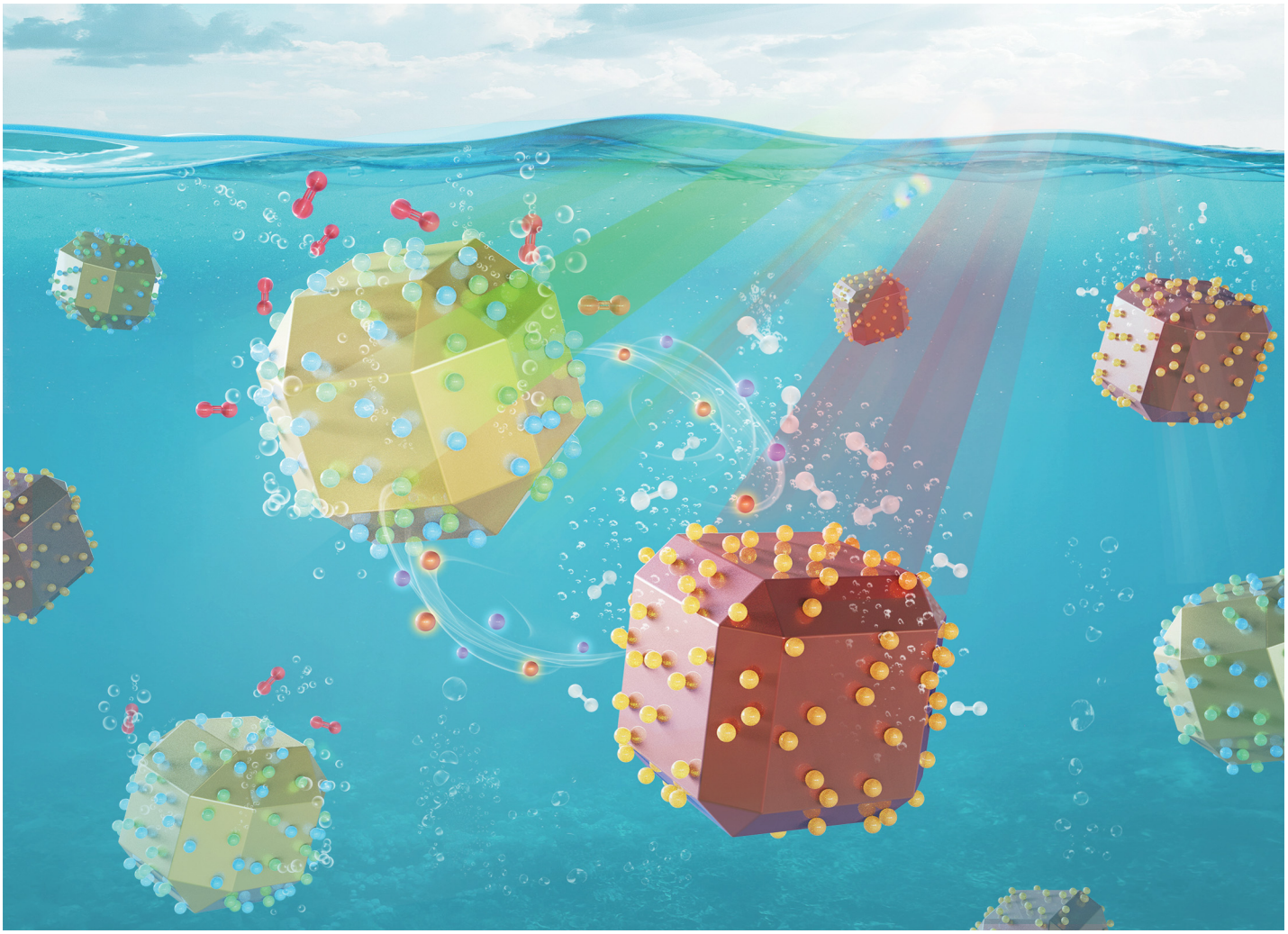

Showcasing research from Professor Domen's laboratory, Research Initiative for Supra-Materials, Shinshu University, Nagano, Japan and Office of University Professors, The University of Tokyo, Tokyo, Japan

Zr-doped $BaTaO_2N$ photocatalyst modified with Na–Pt cocatalyst for efficient hydrogen evolution and Z-scheme water splitting

Direct decomposition of water into hydrogen and oxygen using particulate photocatalysts is a simple and cost-effective approach towards renewable solar hydrogen production on a large scale. We have realized a Z-scheme water splitting system that can operate under visible light at wavelengths up to 520 nm. The Z-scheme system comprises a modified $BaTaO_2N$ as a hydrogen evolution photocatalyst, $BiVO_4$ as an oxygen evolution photocatalyst, and $[Fe(CN)_6]^{3-/4-}$ as a redox mediator. We describe how the performance of $BaTaO_2N$ and associated Z-scheme system can be upgraded.

As featured in:

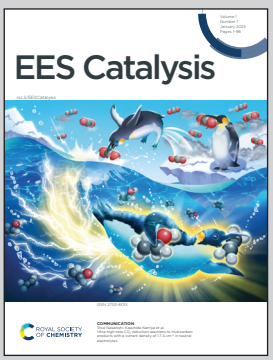

See Kazunari Domen *et al.*, *EES Catal.*, 2023, **1**, 26.

ROYAL SOCIETY OF CHEMISTRY

rsc.li/EESCatalysis

Registered charity number: 207890

EES Catalysis

PAPER

View Article Online
View Journal | View Issue

Cite this: *EES Catal.*, 2023, 1, 26

Zr-doped $BaTaO_2N$ photocatalyst modified with Na–Pt cocatalyst for efficient hydrogen evolution and Z-scheme water splitting†

Huihui Li,[ab] Junie Jhon M. Vequizo,[b] Takashi Hisatomi,[bc] Mamiko Nakabayashi,[d] Jiadong Xiao,[b] Xiaoping Tao,[b] Zhenhua Pan,[b] Wenpeng Li,[e] Shanshan Chen,[f] Zheng Wang,[g] Naoya Shibata,[d] Akira Yamakata,[h] Tsuyoshi Takata[b] and Kazunari Domen *[bi]

Received 26th August 2022,
Accepted 6th November 2022

DOI: 10.1039/d2ey00031h

rsc.li/eescatalysis

$BaTaO_2N$ exhibits hydrogen evolution activity under visible light with wavelengths up to 650 nm and is applicable to Z-scheme overall water splitting (ZOWS). However, the insufficient activity and selectivity of $BaTaO_2N$ in the presence of redox mediators limit the efficiency of this process. Herein, we report the use of modified $BaTaO_2N$ as a hydrogen evolution photocatalyst in combination with $BiVO_4$ and $[Fe(CN)_6]^{3-/4-}$ as the oxygen evolution photocatalyst and redox mediator, respectively. Zr-doped $BaTaO_2N$ ($BaTaO_2N$:Zr) synthesized by flux-assisted thermal nitridation and decorated with Na and Pt (Na–Pt) as cocatalysts was found to provide higher hydrogen evolution activity than undoped $BaTaO_2N$. Zr doping extended the lifetime of electrons in the $BaTaO_2N$ and promoted electron injection into the Na–Pt cocatalysts. Consequently, Na–Pt/$BaTaO_2N$:Zr modified with Cr_2O_3 to suppress reverse reactions evolved hydrogen from an aqueous $K_4[Fe(CN)]_6$ solution. Optimizing the $BaTaO_2N$ photocatalyst and the reaction conditions provided a ZOWS system capable of operating under visible light at wavelengths up to 520 nm. This work indicates that ZOWS systems operable under visible light can be constructed based on detailed investigations of photocatalysts, cocatalysts and redox mediators.

Broader context

Direct decomposition of water into hydrogen and oxygen using particulate photocatalysts is a simple and cost-effective approach towards renewable solar hydrogen production on a large scale. Z-scheme overall water splitting (ZOWS) comprising two-step excitation of a hydrogen evolution photocatalyst (HEP) and an oxygen evolution photocatalyst (OEP) has attracted significant interest, because narrow bandgap photocatalysts can be applied to this process if these materials are active during either the hydrogen or oxygen evolution reactions. However, the past ZOWS systems mostly used wide bandgap semiconductors as either HEPs or OEPs, restricting the use of long-wavelength visible light. This work extends the wavelength range of visible light that can be used for ZOWS by improving the performance of a narrow bandgap oxynitride ($BaTaO_2N$) as the HEP and by selecting an appropriate redox couple for electron transfer. This represents an essential advance towards achieving the solar energy conversion efficiency required for practical photocatalytic hydrogen production. The practice of comprehensive refinement of narrow bandgap oxynitride photocatalysts, cocatalysts, and redox mediators effective for ZOWS will guide the research and development of photocatalytic solar hydrogen production.

[a] *School of Materials and Energy, Lanzhou University, 222 South Tianshui Road, Lanzhou 730000, China*
[b] *Research Initiative for Supra-Materials, Interdisciplinary Cluster for Cutting Edge Research, Shinshu University, Nagano-shi, Nagano 380-8553, Japan. E-mail: domen@shinshu-u.ac.jp*
[c] *PRESTO, JST, 4-17-1 Wakasato, Nagano-shi, Nagano 380-8553, Japan*
[d] *Institute of Engineering Innovation, The University of Tokyo, Tokyo 113-8656, Japan*
[e] *Department of Science and Technology, Graduate School of Medicine, Science and Technology, Shinshu University, 4-17-1 Wakasato, Nagano 380-8553, Japan*
[f] *School of Materials Science and Engineering & National Institute for Advanced Materials, Nankai University, Tianjin 300-350, China*
[g] *Research Center for Eco-Environmental Sciences, Chinese Academy of Sciences, Beijing 100085, China*
[h] *Faculty of Natural Science and Technology, Okayama University, 3-1-1, Tsushima-naka, Kita-ku, Okayama, Japan*
[i] *Office of University Professors, The University of Tokyo, 2-11-16 Yayoi, Bunkyo-ku, Tokyo 113-8656, Japan*

† Electronic supplementary information (ESI) available: Characterization results including those obtained using ICP-OES and N–O analysis; photocatalytic HER data. See DOI: https://doi.org/10.1039/D2EY00031H

Introduction

Z-scheme overall water splitting (ZOWS) comprising two-step excitation of a H_2-evolving photocatalyst (HEP) and O_2-evolving photocatalyst (OEP) has attracted significant interest as a means of harvesting solar energy. Narrow-bandgap materials can be applied to this process if these compounds are active during either the hydrogen or oxygen evolution reactions, and photocatalyst sheets have exhibited efficient scalable ZOWS.[1] The use of p-type semiconductors as HEPs is likely to be essential in the sheet system because the ZOWS mechanism is similar to that for photoelectrochemical cells. Many Cu-based chalcogenides are narrow-bandgap p-type semiconductors, but improving the durability and efficiency of such materials in ZOWS remains challenging.[2,3] In contrast, ZOWS systems based on a suspended HEP and OEP together with ionic electron mediators can operate even when both the HEP and OEP are n-type semiconductors. This is possible because charge transfer between the HEP and OEP can occur *via* photocatalytic reactions of mediator ions instead of at junctions between bulk solid materials.[4–8] Many ZOWS systems have been reported to date. As an example, Qi *et al.* demonstrated a ZrO_2/TaON–$[Fe(CN)_6]^{3-/4-}$–$BiVO_4$ system.[9] The ZrO_2/TaON and $BiVO_4$ photocatalysts can utilize visible light up to 500 and 520 nm, respectively. However, achieving the target solar-to-hydrogen energy conversion efficiency (STH) of 5% or greater required for practical photocatalytic hydrogen production will necessitate the utilization of materials capable of using solar radiation at wavelengths above 530 nm for ZOWS.

$BaTaO_2N$ has an absorption edge wavelength of 650 nm and so is a promising candidate for photocatalytic water splitting under visible light.[10–15] Single-crystalline particulate $BaTaO_2N$ can be obtained by RbCl flux-assisted nitridation.[16] When loaded with a Pt cocatalyst decorated with Na, this compound exhibits excellent hydrogen evolution activity from aqueous methanol solutions, while unmodified $BaTaO_2N$ is inactive.[17] The addition of Na ensures wide dispersion of the Pt nanoparticles during the hydrogen reduction treatment and these highly-dispersed nanoparticles effectively catalyze the hydrogen evolution reaction (HER) on the $BaTaO_2N$. Domen *et al.* reported ZOWS using $BaTaO_2N$ as the HEP, WO_3 as the OEP and IO_3^-/I^- as the ionic shuttle.[16,17] Despite the ability of $BaTaO_2N$ to utilize visible light, the use of WO_3, which has a wide bandgap, restricts the use of wavelengths above 450 nm by this system. Therefore, it would be an important breakthrough to combine $BaTaO_2N$ with OEPs having narrower bandgaps, such as $BiVO_4$.[18] Unfortunately, the low activity of $BaTaO_2N$ in the presence of reversible redox mediators hampers the realization of such ZOWS systems.

Doping is a simple but effective means of tuning the properties of photocatalysts so as to improve their activity. In the case of $BaTaO_2N$, doping with Zr tends to enhance performance by suppressing the formation of Ta^{3+} defects during the thermal nitridation process. Abe *et al.* demonstrated a negative shift in the photoanodic current onset potential when using Zr-doped $BaTaO_2N$.[19] Our own group also synthesized $BaZrO_3$–$BaTaO_2N$ solid solutions that exhibited improved photocatalytic hydrogen evolution from water under visible light.[20] Accordingly, it is expected that the hydrogen evolution activity of $BaTaO_2N$ synthesized using nitridation in conjunction with a RbCl flux could be improved by doping with Zr. Another important consideration related to ZOWS systems is the ionic electron mediator, which can induce backward reactions. It is therefore important to improve not only the photoreduction activity but the selectivity for the HER associated with the reduction of the ionic electron mediator. This can be accomplished by surface modification of the $BaTaO_2N$ photocatalyst to control the reaction selectivity.

The present work devised an efficient ZOWS system based on Zr-doped $BaTaO_2N$ (denoted herein as $BaTaO_2N$:Zr) as the HEP combined with $BiVO_4$ modified with Au and CoO_x (denoted as CoO_x/Au/$BiVO_4$) as the OEP and $[Fe(CN)_6]^{3-}$/$[Fe(CN)_6]^{4-}$ as the redox mediator.[9] The $BaTaO_2N$:Zr photocatalyst was additionally loaded with a Pt cocatalyst together with Na, as well as with Cr_2O_3.[21] The resulting ZOWS system (denoted as Cr_2O_3/Na–Pt/$BaTaO_2N$:Zr–$[Fe(CN)_6]^{3-/4-}$–CoO_x/Au/$BiVO_4$) exhibited stable H_2 and O_2 evolution at the expected stoichiometric molar ratio during a 30 h trial under simulated sunlight with a STH of 0.022%. The effects of the Zr doping, Na–Pt cocatalyst loading and Cr_2O_3 coating on the ZOWS activity of this material were evaluated.

Results and discussion

Cation-doped $BaTaO_2N$ was prepared *via* the thermal nitridation of a mixture of the corresponding starting materials with an RbCl flux. The effect of doping was investigated by assessing the hydrogen evolution activity of doped $BaTaO_2N$ in an aqueous methanol solution under visible light after loading the Na–Pt cocatalysts. As shown in Fig. 1a, Zr doping enhanced the hydrogen evolution activity of the $BaTaO_2N$ in aqueous methanol while the other dopants investigated in this work actually lowered the activity. Zr^{4+} has the closest valency to Ta^{5+} and the disturbance of the anion compositions by cationic doping would be minimum, which may account for the lower hydrogen evolution reaction activity. On this basis, the optimal Zr doping amount was also investigated. The incorporation of 1% Zr in the $BaTaO_2N$ enhanced the photocatalytic H_2 evolution activity to the greatest extent while higher doping levels reduced the activity (Fig. 1b).

Fig. 2a presents powder XRD patterns obtained from crystals of $BaTaO_2N$:Zr with Zr/Ta = 0, 0.01 and 0.1. The major product in all cases was evidently a perovskite-type material based on a comparison with the standard JCSD pattern for bulk $BaTaO_2N$.[17] However, some small peaks ascribed to Ta_3N_5 were observed even in the pattern for the undoped $BaTaO_2N$. The formation of Ta_3N_5 in the undoped $BaTaO_2N$ was attributed to a loss of barium through volatilization during the high-temperature nitridation process.[22] Upon adding Zr, a larger amount of Ta_3N_5 was generated as a by-product because Zr^{4+} ions were substituted into the Ta^{5+} sites and a corresponding

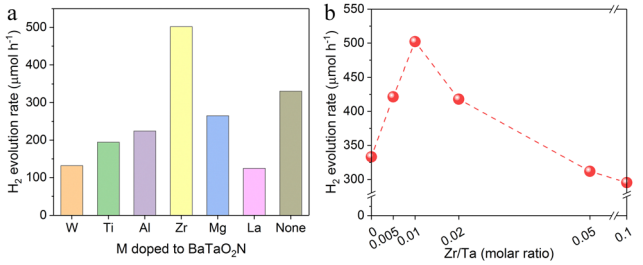

Fig. 1 Photocatalytic H_2 evolution rates obtained for (a) Na–Pt/$BaTaO_2N$ doped with various cations (M) with a M/Ta ratio of 0.01 and (b) Na–Pt/$BaTaO_2N$:Zr with different Zr/Ta molar ratios in an aqueous solution containing methanol (15 vol%). Reaction conditions: 0.23 wt% Na 0.3 wt% Pt/$BaTaO_2N$ photocatalyst, 100 mg; 15 vol% aqueous methanol solution, 150 mL; light source, 300 W Xenon lamp equipped with a cut-off filter (420 nm < λ < 800 nm). Reaction system, Pyrex top-illuminated vessel connected to a closed gas-circulation system with a 10 kPa Ar background pressure.

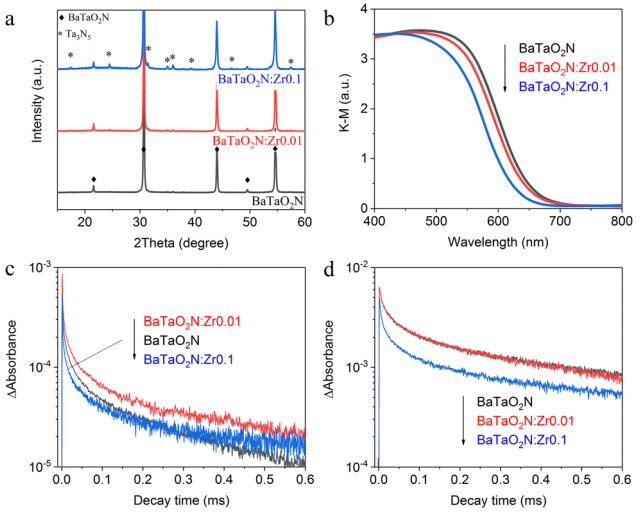

Fig. 2 (a) XRD patterns, (b) DRS spectra, and TAS decays probed at (c) 5000 cm^{-1} (2000 nm; corresponding to electron dynamics) and (d) 15 400 cm^{-1} (649 nm; corresponding to hole dynamics) with excitation at 470 nm for $BaTaO_2N$, $BaTaO_2N$:Zr0.01 and $BaTaO_2N$:Zr0.1.

amount of Ta_2O_5 was segregated and nitrided into Ta_3N_5. The deficiency of barium species with respect to the B-site elements (tantalum and zirconium) was further confirmed by chemical composition analysis (Table S1, ESI†). The Ba/(Ta + Zr) atomic ratio was found to decrease from 1.01 in $BaTaO_2N$ to 0.95 and 0.88 in $BaTaO_2N$:Zr0.01 and $BaTaO_2N$:Zr0.1, respectively. The specific surface areas of undoped $BaTaO_2N$ and $BaTaO_2N$:Zr0.01 were 2.3 and 2.9 $m^2\ g^{-1}$, respectively, suggesting a decrease in the average particle size of $BaTaO_2N$ by Zr doping. This may partly account for the enhancement in the photocatalytic H_2 evolution activity at the low doping amount. Notably, the Zr/Ta ratio in the nitrided products was virtually the same as that in the corresponding starting materials. This result indicates that the added Zr species were not lost during the flux-assisted nitridation and subsequent rinsing processes. Despite the substitution of the lower valence element Zr for Ta, the O/(N + O) molar ratio was unchanged, possibly as a consequence of the formation of Ta_3N_5 (as was indicated by the XRD data). A broad absorption peak in the range of 700–750 nm, characteristic of Ta_3N_5, was not observed in the DRS spectra (Fig. 2b). However, the addition of Zr shifted the light absorption onset to shorter wavelengths with increasing concentration. Doping with lower valence cations results in exchange of nitride ions with oxide ions, decreasing the nitride ion content of the material to maintain the charge neutrality. As a result, the band gap was widened by doping Zr.

The effect of zirconium doping on the dynamics of photogenerated electrons and holes was studied by TAS. Fig. 2c and d provide transient absorption intensity profiles acquired at 5000 cm^{-1} (2000 nm) and 15 400 cm^{-1} (649 nm), respectively. These data reflect the dynamics of the intraband transitions of free and/or shallowly trapped electrons and photoexcited holes, respectively.[23,24] The addition of 1 mol% Zr evidently increased the lifetime of shallowly trapped electrons, in agreement with earlier work by Hojamberdiev *et al.*,[25] but had no appreciable effect on the dynamics of trapped holes. Doping with lower valence cations may suppress the formation of reduced Ta species acting as recombination centers. However, according to the Ta 4f XPS analysis, the chemical states of Ta species were not appreciably changed by Zr-doping, probably due to the low dopant concentration (Fig. S1, ESI†). In-depth analysis of semiconducting properties and defects of particulate oxynitride materials will be required to clarify the physicochemical origin for the prolonged electron lifetime. In contrast, doping with 10 mol% Zr accelerated the decay of both electrons and holes. It is likely that the formation of Ta_3N_5 impurities, which typically have short carrier lifetimes, promoted charge recombination in the specimens.[26] This effect would explain why excessive Zr doping lowered the H_2 evolution activity.

Fig. 3 shows a TEM image of a crystal of the cocatalyst-loaded $BaTaO_2N$:Zr0.01, which exhibited the best H_2 evolution activity. A nearly cubic particle with 100–300 nm in size with clear facets can be seen. Note that rod-like particles typically formed by Ta_3N_5 crystals were not observable due to the low

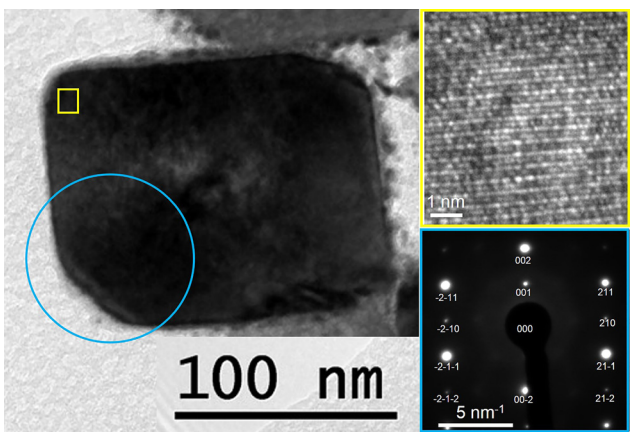

Fig. 3 TEM, HRTEM (inset) and SAED (inset) images of the cross-section of a Cr_2O_3/Na–Pt loaded $BaTaO_2N$:Zr0.01 sample.

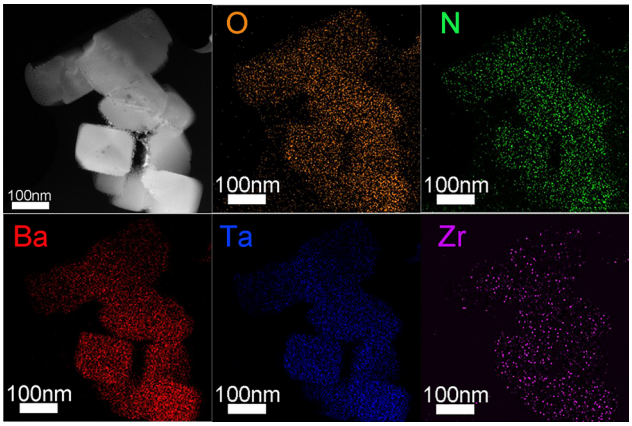

Fig. 4 ADF-STEM image and corresponding STEM-EDS elemental maps of the cross-section of a Cr_2O_3/Na–Pt loaded $BaTaO_2N$:Zr0.01 sample.

amount. The well-defined SAED pattern with no additional diffraction spots (inset to Fig. 3) and the clear lattice fringes observed by HRTEM (inset to Fig. 3) indicate that these $BaTaO_2N$:Zr0.01 particles were single crystals. Elemental mapping of the cross section of a $BaTaO_2N$:Zr0.01 sample with STEM-EDS (Fig. 4) confirmed that the Zr dopant was not segregated from the $BaTaO_2N$ particles. Fig. 4 also shows that the other four elements (Ba, Ta, O and N) were uniformly distributed throughout the $BaTaO_2N$:Zr crystals. These results indicate the homogeneous composition and single-crystalline nature of the $BaTaO_2N$:Zr0.01 crystals.

TAS was also used to examine the effect of zirconium doping on the interaction of the photocatalyst and the Na–Pt cocatalyst (Fig. 5a and b). The addition of the Na–Pt cocatalyst to the $BaTaO_2N$ was found to accelerate the decay of electrons while inhibiting that of holes, similar to the findings of our previous work.[17] This effect occurred because the Na–Pt cocatalyst captured electrons in the $BaTaO_2N$. Interestingly, the acceleration of the electron decay following cocatalyst loading was stronger in the case of the $BaTaO_2N$:Zr0.01, suggesting that electron injection into the Na–Pt cocatalyst was promoted by Zr doping. However, the decay of holes was not retarded appreciably. Zr doping may induce deep-trapping and quenching of photoexcited holes by modifying the anion composition that, in turn, affects the valence band structure of the $BaTaO_2N$.

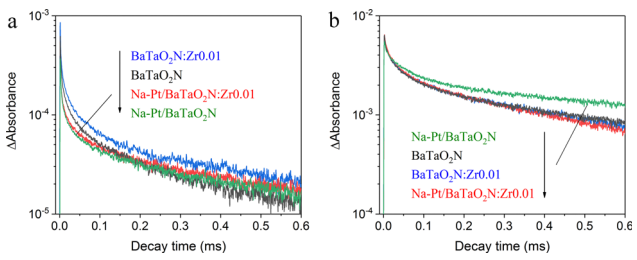

Fig. 5 TAS decays probed at (a) 5000 cm^{-1} (2000 nm; corresponding to electron dynamics) and (b) 15400 cm^{-1} (649 nm; corresponding to hole dynamics) with excitation at 470 nm for $BaTaO_2N$:Zr0.01 and $BaTaO_2N$ before and after the addition of Na–Pt cocatalysts.

Additional in-depth spectroscopic investigations will be required to better explain the TAS observations in the present work.

The hydrogen evolution activity of a HEP in an aqueous solution containing an ionic redox mediator depends on the characteristics of the mediator, such as the redox potential, number of electrons involved in the redox reaction, and adsorption properties.[9] Thus, an appropriate redox mediator for the present ZOWS system was determined by experimental screening. The hydrogen evolution activities of $BaTaO_2N$:Zr0.01 samples loaded with the Na–Pt cocatalyst followed by the photodeposition of Cr_2O_3 from aqueous $K_4[Fe(CN)_6]$, NaI or $FeCl_2$ solutions were evaluated. Here, Cr_2O_3 was employed to suppress backward reactions (*i.e.*, the reduction of oxidized forms of the redox shuttle).[27] As seen in Fig. 6a, the Cr_2O_3/Na–Pt/$BaTaO_2N$:Zr0.01 was almost inactive in aqueous solutions containing I^- or Fe^{2+} shuttle ions, while the same photocatalyst exhibited decent activity when $[Fe(CN)_6]^{4-}$ was employed as the electron donor. The $[Fe(CN)_6]^{3-}/[Fe(CN)_6]^{4-}$ redox couple has a more negative redox potential than the IO_3^-/I^- or Fe^{3+}/Fe^{2+} redox mediators.[9] As a result, photogenerated holes could be transferred from the valence band of the $BaTaO_2N$:Zr0.01 to the $[Fe(CN)_6]^{4-}$ ions more efficiently. In addition, the $[Fe(CN)_6]^{3-}/[Fe(CN)_6]^{4-}$ redox couple works in less extreme pH environments (pH 6–7) than the Fe^{3+}/Fe^{2+} mediator (pH 2–3, at which Cr_2O_3 is unstable). The former couple is also cycled by accepting/donating one electron instead of multiple electrons such as the six electrons required by the IO_3^-/I^- shuttle. These features allowed the Cr_2O_3/Na–Pt/$BaTaO_2N$:Zr0.01 to evolve hydrogen efficiently and steadily, and so the $[Fe(CN)_6]^{3-}/[Fe(CN)_6]^{4-}$ redox shuttle shows promise as a component of ZOWS systems.

Pt nanoparticles were well used as a cocatalyst for hydrogen evolution.[28,29] Note that it was important to apply a Cr_2O_3 layer to the Na–Pt nanoparticles to suppress backward reactions during the HER. As shown in Fig. 6b, without Cr_2O_3 deposition, hydrogen evolution ceased after a few hours due to the progression of backward reactions. With the optimal amount of

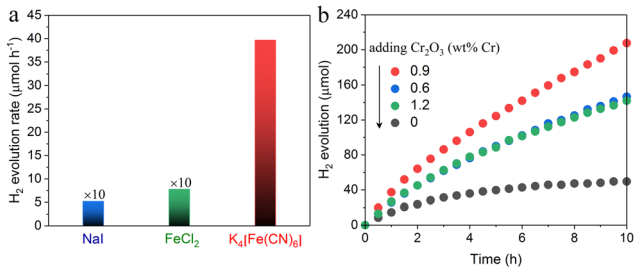

Fig. 6 (a) Photocatalytic H_2 evolution activities of Cr_2O_3/Na–Pt/$BaTaO_2N$:Zr0.01 (100 mg) in aqueous solutions of NaI, $FeCl_2$ and $K_4[Fe(CN)_6]$ (150 mL, 2 mM each) with pH values of 6–7, 2.3 and 6, respectively. (b) Time courses of H_2 evolution over Cr_2O_3/0.23 wt% Na 0.3 wt% Pt/$BaTaO_2N$:Zr0.01 (100 mg) with varying amounts of Cr in an aqueous 50 mM sodium phosphate buffer solution at pH 6 (150 mL) containing 6 mM $K_4[Fe(CN)_6]$. Light source: 300 W xenon lamp ($420\ nm < \lambda < 800\ nm$).

Cr_2O_3, the H_2 evolution performance of the Na–Pt/$BaTaO_2N$:Zr0.01 was promoted because the access of $[Fe(CN)_6]^{3-}$ to the Na–Pt cocatalyst was suppressed.[30] The optimum amount of Cr based on photodeposition was found to be 0.9 wt% with respect to the photocatalyst mass. Greater amounts of Cr actually lowered the hydrogen evolution activity because of the excessive photodeposition of Cr_2O_3 in the presence of methanol. The action spectrum of a Cr_2O_3/Na–Pt/$BaTaO_2N$:Zr0.01 photocatalyst for the hydrogen evolution reaction from aqueous $K_4[Fe(CN)_6]$ solution is provided in Fig. S2 (ESI†). The photocatalyst exhibited the hydrogen evolution activity up to 640 nm, which was consistent with the absorption edge of the material. The AQY at 420 nm was measured to be 0.4%.

Fig. 7 provides ADF-STEM, TEM, and STEM-EDS elemental maps of $BaTaO_2N$:Zr0.01 loaded with 0.23 wt% Na 0.3 wt% Pt and Cr_2O_3 (0.9 wt% Cr). The loading of Pt nanoparticles along with Na was studied in our recent work.[17] According to our previous work, the Pt nanoparticles in this sample had sizes in the range of 2–8 nm. The addition of Na improved the dispersion and structural stability of the Pt cocatalyst, although some cocatalyst particles are seen to have aggregated to form larger secondary particles on the edges of the $BaTaO_2N$ crystal. Na species were not observed because of the low loading amount and the poor sensitivity of EDS for this element. The Cr species appeared to be present in the same positions as the Pt, suggesting the formation of a layer of Cr_2O_3 covering the Pt nanoparticles as in earlier reports,[21] but were distributed over a somewhat wider area.

The $BaTaO_2N$:Zr0.01 photocatalyst loaded with Cr_2O_3/Na–Pt cocatalysts was found to function as a HEP in a ZOWS system in combination with CoO_x/Au/$BiVO_4$ as the OEP and $[Fe(CN)_6]^{3-}$/$[Fe(CN)_6]^{4-}$ as a redox mediator (Fig. 8), whereas the amounts of gaseous products were below the detection limits in the absence of the redox mediator. The same HEP and OEP showed H_2 and O_2 evolution activities from aqueous solutions containing the corresponding redox mediators, respectively (Fig. S3, ESI†). These observations indicate the occurrence of Z-scheme *via* the electron transfer mediated by the $[Fe(CN)_6]^{3-}$/$[Fe(CN)_6]^{4-}$ redox couple. The ZOWS performance of this system was examined under simulated sunlight with evacuation of the test apparatus followed by the reintroduction of Ar to 10 kPa at 10 h intervals. Both H_2 and O_2 were evolved at a molar ratio close to the 2 : 1 stoichiometric ratio, and the STH of this redox-mediated ZOWS system was determined to be 0.022% in the initial run. The AQY values at 420 nm and 520 nm under monochromatic light were 1.5% and 0.2% respectively (Fig. S4, ESI†). Compared with the previously reported $BaTaO_2N$-WO_3 ZOWS system, this system using $BiVO_4$ instead of WO_3 was able to harvest longer-wavelength visible light up to approximately 520 nm. This performance was enabled by doping with 1 mol% Zr, which promoted H_2 evolution on the $BaTaO_2N$, as well as by the modification of the Na–Pt cocatalyst with Cr_2O_3 to inhibit reverse reactions and the use of $[Fe(CN)_6]^{3-}$/$[Fe(CN)_6]^{4-}$ as a suitable redox mediator.

The H_2 evolution rate obtained for the Cr_2O_3/Na–Pt modified $BaTaO_2N$:Zr0.01 in an aqueous $[Fe(CN)_6]^{4-}$ solution (37 μmol h^{-1}; Fig. 6) was slightly lower than the O_2 evolution rate for CoO_x/Au/$BiVO_4$ in a $[Fe(CN)_6]^{3-}$ solution (51 μmol h^{-1}; Fig. S3, ESI†). These data indicate that the rate-determining component of this ZOWS system was the Cr_2O_3/Na–Pt/$BaTaO_2N$:Zr0.01 photocatalyst. In fact, the present system using Cr_2O_3/Na–Pt/$BaTaO_2N$:Zr as the HEP showed inferior AQY and STH values compared with an earlier system using $RhCrO_x$/ZrO_2/TaON.[9] Thus, it is still necessary to improve the preparation of the $BaTaO_2N$:Zr so that more photoexcited charge carriers become available at the surface and to enhance the injection of electrons into the cocatalysts. The present ZOWS system was also found to lose 27% of its original activity when reused, unlike a previously reported system using ZrO_2/TaON loaded with a $Rh_{2-y}Cr_yO_3$ cocatalyst as the HEP.[9] The evolution

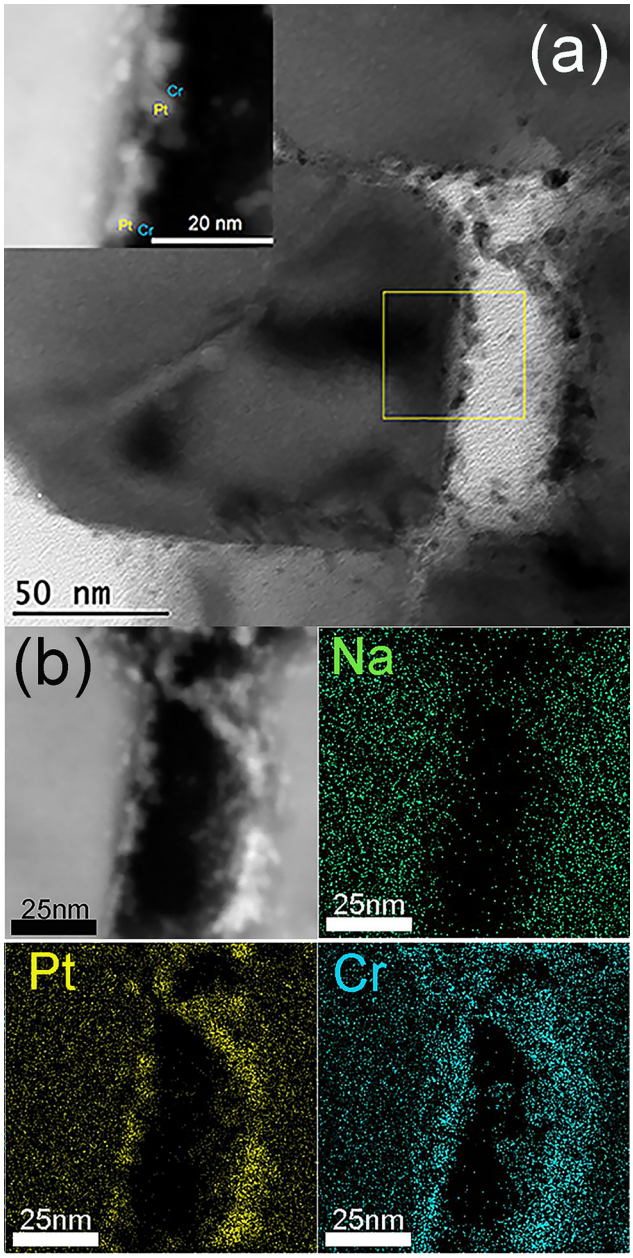

Fig. 7 (a) TEM and ADF-STEM (inset) images and (b) ADF-STEM image along with STEM-EDS elemental maps of the cross-section of a 0.9 wt% Cr_2O_3/0.23 wt% Na 0.3 wt% Pt/$BaTaO_2N$:Zr0.01 sample.

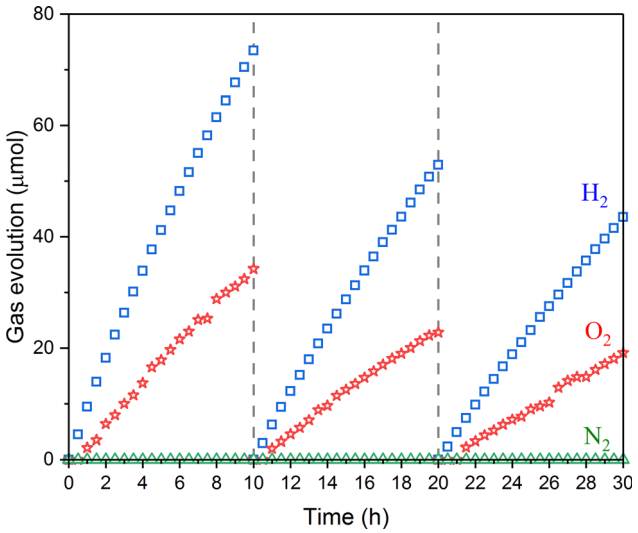

Fig. 8 Time courses of gas evolution during the ZOWS reaction using 70 mg of Cr_2O_3/Na–Pt/$BaTaO_2N$:Zr0.01 as the HEP under simulated sunlight. Conditions: 0.9 wt% Cr_2O_3/0.23 wt% Na 0.3 wt% Pt/$BaTaO_2N$:Zr0.01 as the photocatalyst; 0.5 wt% CoO_x/0.2 wt% Au/$BiVO_4$, 100 mg; 150 mL 25 mM sodium phosphate buffer solution (pH 6) containing $K_4[Fe(CN)_6]$ (6 mM) under simulated sunlight (AM 1.5G, 92 mW cm^{-2}, 5.5 × 5.5 cm). Reaction system: Pyrex top-illuminated vessel connected to a closed gas-circulation system, 10 kPa Ar background atmosphere.

of N_2 was not detected and thus deterioration of the $BaTaO_2N$:Zr0.01 photocatalyst during the 30 h trial was likely negligible. The XRD pattern of the Cr_2O_3/Na–Pt/$BaTaO_2N$:Zr0.01 photocatalyst was also not changed appreciably during the hydrogen evolution reaction (Fig. S5A, ESI†). Therefore, the activity loss was presumably a result of the degradation of the Cr_2O_3/Na–Pt cocatalyst. Degradation of the hydrogen evolution activity of Na–Pt/$BaTaO_2N$ was also observed in our previous work.[17] XPS analysis of the Cr_2O_3/Na–Pt/$BaTaO_2N$:Zr0.01 photocatalyst before and after a ZOWS reaction suggests that the $BaTaO_2N$:Zr0.01 photocatalyst was apparently intact while the Pt cocatalyst was slightly oxidized during the reaction (Fig. S5, ESI†). This may be associated with the degradation of the HER and ZOWS activities. Our previous work showed that coloading of an appropriate water oxidation cocatalyst can improve the durability of the cocatalyst by reducing the probability of hole injection into the hydrogen evolution cocatalyst.[31,32] At present, it is difficult to coload $BaTaO_2N$ with hydrogen evolution cocatalysts and oxygen evolution cocatalysts without sacrificing photocatalytic activity because of the insufficient reactivity and stability of the materials. The development of new technologies for the preparation and modification of narrow-bandgap particulate oxynitride photocatalysts will be vital to the future design of efficient solar-to-chemical energy conversion processes.

Experimental

Synthesis of Zr-doped $BaTaO_2N$

$BaTaO_2N$:Zr samples were synthesized by RbCl (95.0%; FUJIFILM Wako Pure Chemical Corporation) flux-assisted nitridation of a mixture of $ZrO(NO_3)_2{\cdot}2H_2O$ (99.5%; Wako Pure Chemical Industries, Ltd.), $BaCO_3$ (99.9%; Kanto Chemical Co., Inc.) and Ta_2O_5 (99.9%; High Purity Chemicals). Note that all chemicals employed in this study were used directly as received. In a typical synthesis, a certain amount of the mixture (in which the Ba/Ta molar ratio was 1.1 regardless of the Zr/Ta molar ratio) and RbCl were blended thoroughly so that the solute concentration in RbCl flux was 10 mol% and the total mass of solute and RbCl flux was 2 g. The mixture was subsequently heated under an ammonia flow (200 mL min^{-1}) at 1223 K for 8 h, based on a procedure previously reported by our group.[17] The resulting $BaTaO_2N$:Zr was washed with water and dried to give the final product. The $BaTaO_2N$:Zr specimens having varying Zr doping levels are referred to herein as $BaTaO_2N$:Z*r*x, where *x* represents the Zr/Ta molar ratio and ranges from 0 to 0.1. $BaTaO_2N$ specimens doped with other cations at the cation/Ta molar ratio of 0.01 were also prepared for comparison purposes.

Synthesis of $BiVO_4$

$BiVO_4$ was prepared by a hydrothermal procedure.[9] In this process, 5 mmol of NH_4VO_3 (99.0%; FUJIFILM Wako Pure Chemical Corporation) and 5 mmol of $Bi(NO_3)_3{\cdot}5H_2O$ (99.5%; FUJIFILM Wako Pure Chemical Corporation) were dissolved in 50 mL of a 2.0 M nitric acid solution (65%; FUJIFILM Wako Pure Chemical Corporation). The pH of this solution was then adjusted to 1.0 with an ammonia solution (28 wt%; FUJIFILM Wako Pure Chemical Corporation) while stirring the mixture, which generated a light-yellow precipitate. The solution was allowed to age for 2 h with stirring, after which the precipitate was removed and transferred to a Teflon-lined stainless-steel autoclave with a capacity of 100 mL and was hydrothermally treated at 453 K for 11 h. The single phase of diffraction structure of as-prepared $BiVO_4$ (PDF No. 14-0688) was confirmed as shown in Fig. S6 (ESI†).[9]

Deposition of cocatalysts and characterization

The cocatalysts were deposited on the $BaTaO_2N$:Zr by impregnation followed by hydrogen reduction.[17] In a typical process, a 110 mg quantity of $BaTaO_2N$:Zr was immersed in an aqueous solution containing NaOH (0.1 mol L^{-1}; FUJIFILM Wako Pure Chemical Corporation) and $H_2PtCl_6{\cdot}6H_2O$ (98.5%; FUJIFILM Wako Pure Chemical Corporation) as the precursors. The amounts of Pt and Na in the solution were 0.3 and 0.23 wt%, respectively, with respect to the photocatalyst mass. The solution was subsequently heated on a boiling water bath, after which the product was completely dried and then heated at 523 K for 30 min in a flow of 10% H_2 in N_2. The resulting Na–Pt/$BaTaO_2N$:Zr was additionally modified with Cr_2O_3 by photodeposition to suppress backward reactions.[21] This was accomplished by dispersing a quantity of the Na–Pt/$BaTaO_2N$:Zr powder in 100 mL of an aqueous solution of methanol (15 vol%), after which K_2CrO_4 (99.0%; FUJIFILM Wako Pure Chemical Corporation) was added as a Cr^{6+} precursor without pH adjustment. The amount of Cr_2O_3 was equivalent to a loading of 0.9 wt% Cr with respect to the photocatalyst mass. After complete degassing, the suspension was irradiated with

visible light (420 nm $< \lambda <$ 800 nm) for 1 h. The photocatalyst was then removed by filtering, washed with ultrapure water and dried at 313 K under vacuum.

The deposition of Au and CoO_x as reduction and oxidation cocatalysts, respectively, on the $BiVO_4$ was carried out using a stepwise photodeposition process previously reported in the literature.[9] The prepared $BiVO_4$ (150 mg) was dispersed in deionized water to which a specific amount of $HAuCl_4{\cdot}4H_2O$ (99.0%; FUJIFILM Wako Pure Chemical Corporation) was added, equivalent to 0.2 wt% Au relative to the oxide mass. Thereafter, the suspension was irradiated under visible light (420 nm $< \lambda <$ 800 nm) for 1 h, after which the powder was collected by filtration, washed and dried. The as-obtained powder was subsequently loaded with CoO_x (0.5 wt%) by photodeposition. This was accomplished by dispersing the powder in 100 mL of a 50 mM sodium potassium buffer solution (KH_2PO_4, 99.5%; FUJIFILM Wako Pure Chemical Corporation; 44 mM; Na_2HPO_4, 99.0%; FUJIFILM Wako Pure Chemical Corporation; 6 mM) at pH 6.0. A quantity of $K_3[Fe(CN)_6]$ (99.0%; FUJIFILM Wako Pure Chemical Corporation) sufficient to give a concentration of 5 mM was added along with a specific amount of $Co(NO_3)_2{\cdot}6H_2O$ (98.0%; FUJIFILM Wako Pure Chemical Corporation), and the mixture was illuminated for 1 h. The resulting CoO_x/Au/$BiVO_4$ has been shown to work as an excellent OEP in ZOWS systems involving $[Fe(CN)_6]^{3-}$/$[Fe(CN)_6]^{4-}$ as the redox mediator.[9]

X-Ray diffraction (XRD) patterns were acquired using a Rigaku MiniFlex 300 powder diffractometer with a Cu Kα radiation source (λ = 1.5418 Å). The data were analyzed after mathematically removing the contribution from the $K\alpha_2$ line. (Scanning) transmission electron microscopy ((S)TEM) images, energy dispersive X-ray spectroscopy (EDS) mapping images, selected area electron diffraction (SAED) patterns, high-resolution transmission electron microscopy (HRTEM) and annular dark-field (ADF) STEM images were obtained with a JEOL JEM-2800 system equipped with an Oxford Instruments X-MAX 100TLE SDD detector. Diffuse reflectance spectroscopy (DRS) data were acquired with an ultraviolet-visible-near-infrared spectrometer (V-670, JASCO) and converted from reflectance to the Kubelka–Munk function. The Ba, Ta and Zr concentrations in the $BaTaO_2N$:Zr were determined by inductively coupled plasma-atomic emission spectroscopy (ICP-AES; ICPS-8100, Shimadzu). The oxygen and nitrogen contents of the $BaTaO_2N$ were obtained using an oxygen–nitrogen combustion analyzer (Horiba, EMGA-620W). X-Ray photoelectron spectroscopy (XPS) was performed using a PHI Quantera II spectrometer with an Al Kα radiation source. All binding energies were referenced to the C 1s peak (284.8 eV) arising from adventitious carbon. The specific surface area of the samples was calculated from nitrogen adsorption isotherms measured at 77 K with a BELSORP Mini II apparatus (MicrotracBEL) using the Brunauer–Emmett–Teller method.

Transient absorption (TA) spectroscopic measurements were carried out using a Nd:YAG laser system (Continuum, Surelite I; pulse duration: 6 nm) equipped with custom-built spectrometers.[33] The probe beams coming from the halogen lamp (producing visible light) and $MoSi_2$ coil (producing IR light) were used in this measurement for monitoring the absorption signals at 649 and 2000 nm, respectively. In the case of 2000 nm probing, the beam was focused on the sample and was transmitted from the sample and then detected by an mercury cadmium telluride detector. For the 649 nm probing, we used reflection mode, of which the incident probe beam was focused on the sample and then the reflected light from the sample was detected by a Si photodetector. The output electric signal was amplified with an AC-coupled amplifier (Stanford Research Systems, SR560, 1 MHz). The time resolution of the spectrometer was limited to 1 μs by the response of the photodetectors. One thousand responses were accumulated to obtain the transient profiles (that is, the decay curves) at 649 and 2000 nm. The various $BaTaO_2N$:Zr photocatalysts loaded with Na and/or Pt were photoexcited using 470 nm pump pulses with a fluence of 3 mJ $pulse^{-1}$. Each powder sample was fixed on a circular CaF_2 substrate by drop-casting at a density of 1.24 mg cm^{-2}. These TAS analyses were carried out in a vacuum at room temperature.

Photocatalytic H_2 evolution reaction and OWS reaction

The HER over each $BaTaO_2N$ photocatalyst was performed at room temperature in a Pyrex top-irradiation reaction vessel connected to a glass closed gas circulation system. In each trial, a quantity of Na–Pt/$BaTaO_2N$:Zr (100 mg) was dispersed in an aqueous methanol solution (15 vol%, 150 mL) using a magnetic stirrer. The vessel was subsequently evacuated several times to ensure complete air removal. The activity of a photocatalyst can depend on the pressure in the reaction system.[16] Thus, to minimize the effects of changes in pressure resulting from gas evolution and heating of the reaction solution during irradiation, Ar was introduced into the reaction system prior to the reaction to a pressure of approximately 10 kPa. The reaction was initiated by irradiation with a 300 W Xe lamp fitted with a cutoff filter and a dichroic mirror, emitting at 420 nm $< \lambda <$ 800 nm. A flow of cooling water was used to keep the suspension at approximately 283 K throughout the trial. The evolved gases were analyzed by gas chromatography (GC; Shimadzu, GC-8A with a thermal conductivity detector, MS-5 A columns and Ar as the carrier gas). The H_2 evolution rates obtained from aqueous solutions of NaI, $FeCl_2$ and $K_4[Fe(CN)_6]$ and the O_2 evolution rates from an aqueous $K_3[Fe(CN)_6]$ solution were also examined. In each case, an aqueous solution (150 mL) containing the photocatalyst sample (100 mg) was prepared and the pH was adjusted to a specific value for NaI (pH 6–7, 2 mM), $FeCl_2$ (pH 2.3, 2 mM), $K_4[Fe(CN)_6]$ (pH 6, 2 mM) and $K_3[Fe(CN)_6]$ (pH 6, 5 mM). An aqueous HNO_3 solution was used to adjust the pH of the $FeCl_2$ solution while the pH values of the $K_4[Fe(CN)_6]$ and $K_3[Fe(CN)_6]$ solutions were maintained at 6 using a 50 mM sodium potassium buffer solution.

ZOWS reactions were carried out using the same reactor and system described above. In each experiment, Cr_2O_3/Na–Pt/$BaTaO_2N$:Zr (70 mg) and CoO_x/Au/$BiVO_4$ (100 mg), acting as the HEP and OEP, respectively, were suspended in 150 mL of an aqueous sodium potassium buffer solution (pH 6.0, 25 mM)

containing $K_4[Fe(CN)_6]\cdot 3H_2O$ (99.5%; FUJIFILM Wako Pure Chemical Corporation; 6 mM). After complete degassing, Ar gas was introduced to the reaction system to an initial pressure of 10 kPa. Following this, the suspension was irradiated with either a Xe lamp or solar simulator (AM 1.5G, 92 mW cm^{-2}, 5.5 × 5.5 cm), and a cooling water system was employed to maintain the solution at 283 K, as described above. The evolved gases were also analyzed by the same GC instrumentation.

Apparent quantum yield (AQY) and STH

The AQY values for the ZOWS reactions were determined using a procedure similar to that described in our previous paper.[34] The same light source was employed but it was equipped with various band-pass filters. The number of incident photons illuminating the reaction cell was measured using a grating spectroradiometer (LS-100, EKO Instruments). The AQY was then calculated as

$$\text{AQY}\ (\%) = [A \times R]/I \times 100, \quad (1)$$

where R and I represent the amounts of evolved H_2 and O_2 and the number of incident photons per unit time, respectively, and A is the number of electrons and holes consumed to generate one molecule of H_2 and one molecule of O_2. The values of A are 4 and 8 for Z-scheme water splitting based on two-step photoexcitation, respectively. The average of the AQY values calculated for H_2 and O_2 values was adopted.

The STH values for ZOWS reactions under simulated solar radiation were calculated as

$$\text{STH}\ (\%) = (R(H_2) \times \Delta G_r)/(P \times S) \times 100, \quad (2)$$

where $R(H_2)$, ΔG_r, P, and S denote the rate of hydrogen evolution determined from the rate of water splitting during the ZOWS reaction, the Gibbs energy change for the reaction H_2O (l) → H_2 (g) + 1/2 O_2 (g), the energy intensity of the AM 1.5G solar irradiation (92 mW cm^{-2}) and the irradiated sample area (5.5 × 5.5 cm), respectively. The rate of water splitting was assumed to equal the average of the H_2 evolution rate and twice the O_2 evolution rate based on the reaction stoichiometry. The value of ΔG_r used for the calculations was 229 kJ mol^{-1} at 283 K.[34]

Conclusions

This work demonstrated the effective modification of a $BaTaO_2N$ photocatalyst by Zr doping and by incorporating a Na–Pt cocatalyst together with a Cr_2O_3 coating to produce a HEP for ZOWS. Doping with 1 mol% Zr extended the lifetime of electrons and promoted electron injection into the Na–Pt cocatalyst, leading to improved H_2 evolution activity for an aqueous methanol solution under visible light. The Cr_2O_3 coating also allowed the Na–Pt/$BaTaO_2N$:Zr0.01 photocatalyst to evolve H_2 from an aqueous $[Fe(CN)_6]^{3-/4-}$ solution.

A ZOWS system based on Cr_2O_3/Na–Pt/$BaTaO_2N$:Zr0.01 as the HEP, CoO_x/Au/$BiVO_4$ as the OEP and $[Fe(CN)_6]^{3-/4-}$ as redox ions evolved H_2 and O_2 under visible light up to 520 nm. The STH efficiency of this process was 0.022%. This newly developed ZOWS system was able to harvest visible light with longer wavelengths than earlier systems utilizing TaON as the HEP or WO_3 as the OEP. This achievement was made possible by improving the performance of the $BaTaO_2N$ as the HEP and also by the selection of $[Fe(CN)_6]^{3-/4-}$ as an appropriate redox couple. It is therefore important to optimize the photocatalyst, cocatalysts and reaction conditions to enhance the activity of ZOWS systems operating under long-wavelength visible light.

Author contributions

The manuscript was written through contributions of all authors. H. L. designed and performed the experiments, wrote and edited the manuscript. J. J. M. V. acquired the TAS spectra and analyzed these data together with A. Y. T. H. edited the manuscript and discussed the scientific results as a supervisor. M. N. characterized the morphology and composition of each specimen using STEM-EDS and HRTEM together with N. S. J. X., Z. P. W. L. and W. Z. discussed the scientific results. X. T. and S. C. discussed the synthesis of $BiVO_4$. T. T. provided resources as a supervisor. K. D. edited the manuscript and provided resources as a supervisor. All authors have given approval to the final version of the manuscript.

Conflicts of interest

There are no conflicts to declare.

Acknowledgements

This research was supported by the National Natural Science Foundation of China (grant no. 51402139), the China Scholarship Council (grant no. 201906185004 and 202008440289), the Artificial Photo-synthesis Project (ARPChem) of the New Energy and Industrial Technology Development Organization (NEDO), and by JST, PRESTO, Japan (grant no. JPMJPR20T9). Part of this study was supported by the University of Tokyo Advanced Characterization Nanotechnology Platform as part of the Nanotechnology Platform Project sponsored By the Ministry of Education, Culture, Sports, Science and Technology (MEXT), Japan (grant no. JPMXP09A-21-UT-0046). W. L. thanks 2021 MEXT Scholarship with Embassy Recommendation for financial support. The authors thank Ms Michiko Obata of Shinshu University for her assistance during the XPS analyses. The authors thank Dr Taro Yamada, Ms Keiko Kato and Ms Yasuko Kuromiya of the University of Tokyo for their assistance in the ICP-OES and oxygen–nitrogen combustion analyses.

Notes and references

1 Q. Wang, T. Hisatomi, Q. Jia, H. Tokudome, M. Zhong, C. Wang, Z. Pan, T. Takata, M. Nakabayashi, N. Shibata, Y. Li, I. Sharp, A. Kudo, T. Yamada and K. Domen, Scalable water splitting on particulate photocatalyst sheets with a

solar-to-hydrogen energy conversion efficiency exceeding 1%, *Nat. Mater.*, 2016, **15**, 611–615.

2 K. Iwashina, A. Iwase, Y. Ng, R. Amal and A. Kudo, Z-Schematic Water Splitting into H_2 and O_2 Using Metal Sulfide as a Hydrogen-Evolving Photocatalyst and Reduced Graphene Oxide as a Solid-State Electron Mediator, *J. Am. Chem. Soc.*, 2015, **137**, 604–607.

3 S. Chen, J. Vequizo, Z. Pan, T. Hisatomi, M. Nakabayashi, L. Lin, Z. Wang, K. Kato, A. Yamakata, N. Shibata, T. Takata, T. Yamada and K. Domen, Surface Modifications of $(ZnSe)_{0.5}(CuGa_{2.5}Se_{4.25})_{0.5}$ to Promote Photocatalytic Z-Scheme Overall Water Splitting, *J. Am. Chem. Soc.*, 2021, **143**, 10633–10641.

4 J. Nasir, A. Munir, N. Ahmad, T. Haq, Z. Khan and Z. Rehman, Photocatalytic Z-Scheme Overall Water Splitting: Recent Advances in Theory and Experiments, *Adv. Mater.*, 2021, **33**, 2105195.

5 B. Ng, L. Putri, X. Kong, Y. The, P. Pasbakhsh and S. Chai, Z-Scheme Photocatalytic Systems for Solar Water Splitting, *Adv. Sci.*, 2020, **7**, 1903171.

6 Y. Miseki and K. Sayama, Photocatalytic Water Splitting for Solar Hydrogen Production Using the Carbonate Effect and the Z-Scheme Reaction, *Adv. Energy Mater.*, 2019, **9**, 1801294.

7 K. Maeda, Z-Scheme Water Splitting Using Two Different Semiconductor Photocatalyst, *ACS Catal.*, 2013, **3**, 1486–1503.

8 R. Zhang, L. Zhang, Q. Zheng, P. Gao, J. Zhao and J. Yang, Direct Z-Scheme Water Splitting Photocatalyst Based on Two-Dimensional van der Waals Heterostructures, *J. Phys. Chem. Lett.*, 2018, **9**, 5419–5424.

9 Y. Qi, Y. Zhao, Y. Gao, D. Li, Z. Li, F. Zhang and C. Li, Redox-Based Visible-Light-Driven Z-Scheme Overall Water Splitting with Apparent Quantum Efficiency Exceeding 10%, *Joule*, 2018, **2**, 2393–2402.

10 M. Hojamberdiev, K. Yubuta, J. Vequizo, A. Yamakata, S. Oishi, K. Domen and K. Teshima, NH_3-Assisted Flux Growth of Cube-like $BaTaO_2N$ Submicron Crystals in a Completely Ionized Nonaqueous High-Temperature Solution and Their Water Splitting Activity, *Cryst. Growth Des.*, 2015, **15**, 4663–4671.

11 S. Wei, S. Chang, F. Yang, Z. Fu, G. Liu and X. Xu, Stable and efficient solar-driven photoelectrochemical water splitting into H_2 and O_2 based on a $BaTaO_2N$ photoanode decorated with CoO microflowers, *Chem. Commun.*, 2021, **57**, 4412–4415.

12 H. Zhang, S. Wei and X. Xu, Mg modified $BaTaO_2N$ as an efficient visible-light-active photocatalyst for water oxidation, *J. Catal.*, 2020, **383**, 135–143.

13 S. Wei, G. Zhang and X. Xu, Activating $BaTaO_2N$ by Ca modifications and cobalt oxide for visible light photocatalytic water oxidation reactions, *Appl. Catal., B*, 2018, **237**, 373–381.

14 B. Dong, Y. Qi, J. Cui, B. Liu, F. Xiong, X. Jiang, Z. Li, Y. Xiao, F. Zhang and C. Li, Synthesis of $BaTaO_2N$ oxynitride from Ba-rich oxide precursor for construction of visible-light-driven Z-scheme overall water splitting, *Dalton Trans.*, 2017, **46**, 10707–10713.

15 K. Hibino, M. Yashima, T. Oshima, K. Fujii and K. Maeda, Structures, electron density and characterization of novel photocatalysts, $(BaTaO_2N)_{1-x}(SrWO_2N)_x$ solid solutions, *Dalton Trans.*, 2017, **46**, 14947–14956.

16 Z. Wang, Y. Luo, T. Hisatomi, J. Vequizo, S. Suzuki, S. Chem, M. Nakabayashi, L. Lin, Z. Pan, N. Kariya, A. Yamakata, N. Shibata, T. Takata, K. Teshima and K. Domen, Sequential cocatalyst decoration on $BaTaO_2N$ towards highly-active Z-scheme water splitting, *Nat. Commun.*, 2021, **12**, 1005.

17 H. Li, D. Lu, S. Chem, T. Hisatomi, J. Vequizo, J. Xiao, Z. Wang, L. Lin, Q. Xiao, Y. Sun, Y. Miseki, K. Sayama, A. Yamakata, T. Takata and K. Domen, A Na-containing Pt cocatalyst for efficient visible-light-induced hydrogen evolution on $BaTaO_2N$, *J. Mater. Chem. A*, 2021, **9**, 13851–13854.

18 A. Iwase, Y. Udagawa, S. Yoshino, Y. Ng, R. Amal and A. Kudo, Solar Water Splitting under Neutral Conditions Using Z-Scheme Systems with Mo-Doped $BiVO_4$ as an O_2-Evolving Photocatalyst, *Energy Technol.*, 2019, **7**, 1900358.

19 M. Higashi, Y. Yamanaka, O. Tomita and R. Abe, Fabrication of cation-doped $BaTaO_2N$ photoanodes for efficient photoelectrochemical water splitting under visible light irradiation, *APL Mater.*, 2015, **3**, 104418.

20 K. Maeda, D. Lu and K. Domen, Solar-Driven Z-scheme Water Splitting Using Modified $BaZrO_3$-$BaTaO_2N$ Solid Solutions as Photocatalysts, *ACS Catal.*, 2013, **3**, 1026–1033.

21 K. Maeda, K. Teramura, D. Lu, N. Saito, Y. Inoue and K. Domen, Noble-Metal/Cr_2O_3 Core/Shell Nanoparticles as a Cocatalyst for Photocatalytic Overall Water Splitting, *Angew. Chem.*, 2006, **118**, 7970–7973.

22 Y. Luo, Z. Wang, S. Suzuki, K. Yubuta, N. Kariya, T. Hisatomi, K. Domen and K. Teshima, Fabrication of Single-Crystalline $BaTaO_2N$ from Chloride Fluxes for Photocatalytic H_2 Evolution under Visible Light, *Cryst. Growth Des.*, 2020, **20**, 255–261.

23 A. Yamakata and J. Vequizo, Curious Behaviors of Photogenerated Electrons and Holes at the Defects on Anatase, Rutile, and Brookite TiO_2 Powders: A Review, *J. Photochem. Photobiol., C*, 2019, **40**, 234–243.

24 A. Yamakata, J. Vequizo, T. Ogawa, K. Kato, S. Tsuboi, N. Furutani, M. Ohtsuka, S. Muto, A. Kuwabara and Y. Sakata, Core-Shell Double Doping of Zn and Ca on β–Ga2O3 photocatalysts for Remarkable Water Splitting, *ACS Catal.*, 2021, **11**, 1911–1919.

25 M. Hojamberdiev, R. Vargas, Z. Kadirova, K. Kato, H. Sena, A. Krasnov, A. Yamakata, K. Teshima and M. Lerch, Unfolding the Role of B Site-Selective Doping of Aliovalent Cations on Enhancing Sacrificial Visible Light-Induced Photocatalytic H_2 and O_2 Evolution over $BaTaO_2N$, *ACS Catal.*, 2022, **12**, 1403–1414.

26 J. Vequizo, M. Hojamberdiev, K. Teshima and A. Yamakata, Role of CoO_x cocatalyst on Ta_3N_5 photocatalysts studied by transient visible to mid-infrared absorption spectroscopy, *J. Photochem. Photobiol., A*, 2018, **358**, 315–319.

27 M. Yoshida, K. Takanabe, K. Maeda, A. Ishikawa, J. Kubota, Y. Sakata, Y. Ikezawa and K. Domen, Role and Function of Noble-Metal/Cr-Layer Core/Shell Structure Cocatalysts for

Photocatalytic Overall Water Splitting Studied by Model Electrodes, *J. Phys. Chem. C*, 2009, **113**, 10151–10157.

28 L. Lin, Z. Lin, J. Zhang, X. Cai, W. Lin, Z. Yu and X. Wang, Molecular-level insights on the reactive facet of carbon nitride single crystals photocatalysing overall water splitting, *Nat. Catal.*, 2020, **3**, 649–655.

29 M. Liu, C. Wei, H. Zhuzhang, J. Zhou, Z. Pan, W. Lin, Z. Yu, G. Zhang and X. Wang, Fully Condensed Poly (Triazine Imide) Crystals: Extended π-Conjugation and Structural Defects for Overall Water Splitting, *Angew. Chem., Int. Ed.*, 2022, **61**, e202113389.

30 M. Qureshi, T. Shinagawa, N. Tsiapis and K. Takanabe, Exclusive Hydrogen Generation by Electrocatalysts Coated with an Amorphous Chromium-Based Layer Achieving Efficient Overall Water Splitting, *ACS Sustainable Chem. Eng.*, 2017, **5**, 8079–8088.

31 H. Lyu, T. Hisatomi, Y. Goto, M. Yoshida, T. Higashi, M. Katayama, T. Takata, T. Minegishi, H. Nishiyama, T. Yamada, Y. Sakata, K. Asakura and K. Domen, An Al-doped $SrTiO_3$ Photocatalyst maintaining sunlight-driven overall water splitting activity for over 1000 h of constant illumination, *Chem. Sci.*, 2019, **10**, 3196–3201.

32 T. Ohno, L. Bai, T. Hisatomi, K. Maeda and K. Domen, Photocatalytic Water Splitting Using Modified GaN:ZnO Solid Solution under Visible Light: Long-Time Operation and Regeneration of Activity, *J. Am. Chem. Soc.*, 2012, **134**, 8254–8259.

33 A. Yamakata, M. Kawaguchi, T. Nishimura, T. Minegishi, J. Kubota and K. Domen, Behavior and Energy States of Photogenerated Charge Carriers on Pt- or CoO_x-Loaded $LaTiO_2N$ photocatalysts: Time-Resolved Visible to Mid-Infrared Absorption Study, *J. Phys. Chem. C*, 2014, **118**, 23897–23906.

34 Z. Wang, T. Hisatomi, R. Li, K. Sayama, G. Liu, K. Domen, C. Li and L. Wang, Efficiency Accreditation and Testing Protocols for Particulate Photocatalysts toward Solar Fuel Production, *Joule*, 2021, **5**, 344–359.